materials

MDPI

Article

Origin of the Optimization of Photocatalytic Activities for Titanium Oxide Film Modified by an Oxidized Copper Layer

Jian-An Chen, Shu-Min Tsai, Yi-You Hong, Pin-Jyun Shih and Day-Shan Liu *

Institute of Electro-Optical and Materials Science, National Formosa University, Huwei 63201, Taiwan
* Correspondence: dsliu@nfu.edu.tw; Tel.: +886-5-6315665

Abstract

In this study, the surface photocatalytic activity of an anatase–titanium oxide (TiO_x) film was modified by a thin copper (Cu) layer with the subsequential oxidation annealing process. Through this simple annealing process, the photocatalytic activity of the TiO_x/Cu structure to decompose the methylene blue solution and inhibit the growth of *Escherichia coli*. could be optimized. With the help of a study on the conductive type required for the oxidation of a single Cu layer, an *n/p* nanocomposite heterojunction was realized, as this contact system anneals at temperatures of 350 °C and 450 °C. An extra electrical field at the contact interfaces that was be beneficial for separating the photo-generated electron–hole pairs (EHPs) under UV light irradiation was built. The built-in electrical field led to an increase in the structural photocatalytic activity. Moreover, as the *p*-type cuprous oxide (*p*-Cu_2O) structure oxidized by the annealed Cu layer could provide a high conduction band that is offset when in contact with the TiO_x film, the photogenerated EHPs on the TiO_x surface could be separated more effectively. Accordingly, the 350 °C-annealed sample, abundant in the nanocomposite TiO_x/Cu_2O heterojunction which could significantly retard the recombination of photo-generated carriers, corresponded to an increase of about 38% in the photocatalytic activity as compared with the single TiO_x film.

Keywords: photocatalytic activity; TiO_x/Cu structure; antibacterial activity; *n/p* nanocomposite heterojunction; *p*-type cuprous oxide

check for updates

Received: 4 May 2025
Revised: 11 June 2025
Accepted: 13 June 2025
Published: 24 June 2025

Citation: Chen, J.-A.; Tsai, S.-M.; Hong, Y.-Y.; Shih, P.-J.; Liu, D.-S. Origin of the Optimization of Photocatalytic Activities for Titanium Oxide Film Modified by an Oxidized Copper Layer. *Materials* **2025**, *18*, 2993. https://doi.org/10.3390/ma18132993

Copyright: © 2025 by the authors. Licensee MDPI, Basel, Switzerland. This article is an open access article distributed under the terms and conditions of the Creative Commons Attribution (CC BY) license (https://creativecommons.org/licenses/by/4.0/).

1. Introduction

Metal oxide films with controllable conduction and broadband transparency are quite appropriate for using with optical and electrical coatings. Among those coatings, titanium oxide (TiO_x) possesses a high refractive index with wide energy bandgap, making it an ideal candidate to be applied in the laminated optical structure, both at visible wavelengths and, in electronics, as a transparent dielectric layer [1–3]. Moreover, TiO_x has low toxicity and bio-inertness as well as strong redox ability when illuminated by ultraviolet (UV) radiation, leading it to become a valuable surface modification layer in the environmental purification and biomedical engineering applications [4–7]. Redox complexes with strong oxidative and reduction potential, such as hydroxyl radical (·OH), superoxide radical ($\cdot O_2^-$), and hydrogen peroxide (H_2O_2), form on the UV-light-activated TiO_x surface as a consequence of the photo-generated electron–hole pairs (EHPs), reacting with the environmental vapor and oxygen to provide excellent photocatalysis for mineralizing pollutants and inhibiting bacterial growth. Thus far, researchers have sought to achieve a TiO_x film that possesses the anatase crystalline structure with a maximized specific surface area through adequate deposition and/or post-annealing processes that behave as a nanotextured surface [8–10].

In addition to engineering the TiO_x film's crystallinity and surface morphology, researchers have also tried to optimize the photocatalytic activity of the TiO_x film in visible-light wavelengths by doping specific impurities [11–13]. Another effective method for enhancing the photocatalytic activity of a TiO_x film is building a heterojunction structure for inhibiting the recombination of the photo-generated EHPs on the TiO_x film's surface. To achieve this, noble metal that possesses a high Fermi energy level (e.g., Au, Ag, and Pt), serving as a sink for the photo-generated electrons, is applied to create hetero-contact with the TiO_x film [14–16]. In our previous study, a thin Ag layer was deposited onto the TiO_x film to modify the structural photocatalytic activity. It was found that the TiO_x film surface decorated by the Ag nanoparticle achieved by an annealing process under ambient nitrogen possessed the optimal photocatalytic activity [17]. In addition to engineering the hetero-contact by using the noble metal and TiO_x, *p*-type semiconductors oxidized from the d-block transition metals are another promising material for enhancing structural photocatalytic activity that occurs while in contact with a TiO_x film [18–21]. This heterojunction structure realizes the *p*/*n* junction structure, which can build an internal electric field for facilitating the separation of the photo-generated EHPs. Among these structures, *p*-type copper oxide (Cu_xO) is the preferred candidate because the element Cu is one of the most abundant transition metals and is more cost-effective than the noble metals. To obtain the Cu_xO film, the thermal oxidation process on the metallic Cu layer is the simplest and most cost-effective method. Given that, on the thermal oxidized Cu species, *p*-type semiconducting cupric oxide (CuO) and cuprous oxide (Cu_2O) are the main crystalline phases and given the different physical properties in these two *p*-type semiconductors, the content of these two phases (Cu_2O/CuO) in the TiO_x/Cu_xO heterojunction contact system becomes a key issue for influencing the resulting photocatalytic activity. For instance, Kim et al. synthesized a mesoporous copper oxide–titanium oxide nanohybrid structure using a solid-state reaction process. The authors found that post-heated temperatures (200–500 °C) are crucial for the phase transformation of the rutile and anatase TiO_2 structures as well as the oxidation phases of the Cu_2O and CuO structures. The 200 °C-calcined CuO/Cu_2O-TiO_2 nanohybrid structure irradiated by visible light showed optimal photocatalytic activity for decomposing the methyl orange [22]. Yurddaskal et al. prepared Cu_2O and CuO structures from the electroplated Cu coatings on the titanium substrate using thermal annealing in ambient air from 200 °C to 600 °C. They found that the CuO/Cu_2O structures achieved from the 500 °C-annealed process demonstrated the highest photodegradation efficiency for MB solution. The reason for the optimal photocatalytic activity was the enriched surface structure of the CuO phase, which is beneficial for the interfacial charge when transferring and inhibiting the recombination of the photo-generated EHPs [23]. More recently, Sarac et al. produced Cu_xO nanowires from thermal oxidized copper foil at temperatures ranging from 400 °C to 600 °C. The authors subsequently coated the foil with TiO_2 film via the hydrolysis process using a titanium isopropoxide solution to prepare the Cu_xO/TiO_x structure so as to improve the charge separation efficiency under UV-A light irradiation. They found that the photocatalytic activity was highly dependent on the CuO nanowire density, nanowire aspect ratio, and the TiO_2 layered thickness. This Cu_xO nanowire/TiO_2 structure with an optimal photocatalytic performance was obtainable from the 450 °C-annealed Cu_xO nanostructures immersed in 40 mM solution [24].

According to the above-mentioned reports, the photocatalytic performance of the TiO_x/Cu_xO system is deeply correlated to its post-annealing temperatures, which are crucial to the appearance of the *p*-type CuO and Cu_2O phases. Here, with the aim to simplify the fabrication and develop a TiO_x/Cu heterojunction structure without the effect on the substate's scale or shape, we engineered a conventional thin-film deposition method with a post-annealing treatment to achieve the TiO_x/Cu_xO contact system. In order to

accomplish this objective, the TiO_x film with anatase phase that had been affected by the CuO and Cu_2O crystallization by a simple post-oxidation treatment on the evaporated thin Cu layer was carried out and investigated. The corresponding photocatalytic and antibacterial activities were determined as the as-deposited and annealed samples were used to decompose the methylene blue (MB) solution and sterilize *E. coli* while being activated by irradiation using a UV lamp. The chemical bond configurations at the interface of the TiO_x/Cu contact system, as well as the crystalline and phase transformation of the single Cu layer oxidized by the identical annealing process, were comprehensively studied to elucidate the evolutions of the resulting photocatalytic activities. Based on these investigations, the mechanism responsible for the TiO_x/Cu structure through a simple oxidation process that exhibited the optimal photocatalytic activity was conducted. Such a TiO_x/Cu structure, prepared purely by the thin-film deposition technology, has the advantage of thickness uniformity and material consistency over a large area, leading it to become less susceptible to the substrate/device size and shape than similar structures that are reported in the referenced papers.

2. Material Preparation and Experimental Procedure

Amorphous titanium oxide (TiO_x) films with a thickness of 200 nm were deposited onto n-type silicon (100) and quartz substrates, using the plasma enhanced chemical vapor deposition (PECVD) system under an ambient temperature of 200 °C. A titanium tetraisopropoxide [$Ti(OC_3H_7)_4$, TTIP] liquid source [97%, Sigma-Aldrich, Saunt Louis, MO, USA] was utilized as the titanium precursor through a heated bubbling cylinder at 70 °C and carried by nitrogen gas. A vaporized TTIP precursor was mixed with oxygen gas in a cylindrical stainless-steel barrel. All the gas pipelines were heated to 100 °C to prevent the condensation of the precursor and gas mixture. The deposition pressure, rf power, and TTIP/O_2 gas mixture were controlled at 40 Pa, 100 W, and 120/20 sccm, respectively. Detailed deposition parameters and system setup are described elsewhere [25]. The deposited TiO_x film was then annealed at 500 °C for 30 min under ambient oxygen to result in the anatase crystallization [25]. A Cu layer with a thickness of about 10 nm was then evaporated onto the anatase–TiO_x film surface, and sequentially annealed at 250 °C, 350 °C, and 450 °C under ambient oxygen for 1 min. To give an insight into the evolutions of the electrical and crystalline properties of the Cu layer itself, another set of the single Cu layer with a thickness of about 200 nm was directly deposited onto the silicon and glass substrates and then processed by the same rapidly thermal annealing (RTA) treatment at a temperature ranging from 250 °C to 450 °C for 1 min under ambient oxygen.

The film thickness of the TiO_x film, the Cu layer, and the TiO_x/Cu heterojunction structure was measured using a surface profile system (Dektak 6M, Veeco, Plainview, NY, USA) and confirmed by cross-section field emission scanning electron microscope (FE-SEM, JSM-6700F, JEOL, Akishima, Tokyo) images. Surface roughness and morphologies were examined using atomic force microscopy (AFM, DI-3100, Veeco, Plainview, NY, USA) and plane view FE-SEM observations. The optical transmittance of these samples was conducted with a UV–Vis–NIR spectrophotometer (UVD 3500, Labomed, Inc., Los Angeles, CA, USA). The crystallinities of the TiO_x/Cu structures and of the single Cu layer oxidized under the same annealing treatments were analyzed using a grazing incident X-ray diffractometer (GIXRD) at 30 kV and 30 mA using Cu $K_{\alpha 1}$ radiation (D-500, Siemens, Munich, Germany). An X-ray photoelectron spectroscope (XPS) with monochromatic Al $K\alpha$ radiation (PHI Quantera SXM^{TM}, ULVAC-PHI, Chigasaki, Japan) was employed to examine the chemical bond configurations distributed over the interface of the as-deposited and annealed TiO_x/Cu contact systems. Ar^+ sputtering was used to etch the TiO_x/Cu structure to the depth near the contact interface during the XPS measurements. The XPS signal at the

binding energy of 284.6 eV in the C 1*s* core level, which occurred due to the surface hydrocarbon contaminations, served as the reference to predetermine the adequacy of the charge neutralization. The binding energy of the Ti 2*p* core level examined from the single TiO_x film was used as an internal reference signal to calibrate the XPS spectra examined from these TiO_x/Cu structures after etching by the Ar^+ sputtering [26,27]. The electrical properties of the single Cu layer treated by the same RTA process were measured using van der Pauw Hall measurements (Ecopia HMS-5000, Ecopia, Anyang, Republic of Korea) at room temperature. The resulting photocatalytic activities of the as-deposited and annealed TiO_x/Cu structures, as well as the single TiO_x and Cu films, were evaluated from these measurements in order to decolorize an aqueous MB solution (20 mgL^{-1} with a pH value approximately of 7.0 $\pm$ 0.1) at ambient temperature under UV lamp irradiation. The associated antibacterial activities were assessed with a plate-counting method while the samples were used against *E. coli*. Microbiological tests were carried out as the samples were immersed into a nutrient broth, and the initial concentration of the *E. coli* bacteria was adjusted to 1.0×10^6 colony-forming unit (CFU)/mL by dilution. These specimens were then sterilized under UV lamp irradiation for 1 h. Subsequently, 0.1 mL of each dilution was taken and spread on the nutrient agar and then incubated at 37 °C for 24 h. The number of bacterial colonies grown on the plates was counted (in CFU) and photographed. The UV lamp emitted the dominant wavelength of 365 nm with a power density that was controlled at 5 mW/cm^2. The photo-excited currents—generated as the UV lamp irradiated on to the surface of the single TiO_x film and TiO_x/Cu heterojunction structures with the pattern of the interdigital transducer (IDT) electrodes while operated at a controlled bias of 10 V—were also measured using a semiconductor parameter analyzer (HP4156C, Keysight Technology, Santa Clara, CA, USA). Based on the specific analysis of the crystallinity of the single Cu layer annealed by the same oxidation treatment, the mechanism responsible for the changes of the photocatalytic activities for these TiO_x/Cu contact systems treated through the simple annealing process can be elucidated more clearly.

3. Results and Discussions

The optical transmittance of the Cu layer deposited onto the TiO_x film and sequentially treated by an RTA process at temperatures of 250 °C, 350 °C, and 450 °C for 1 min under ambient oxygen, as well as the single TiO_x film, are illustrated in Figure 1. The TiO_x film showed optical transparency, with an average transmittance of about 84% around the visible wavelength (from 400 nm to 700 nm). Beyond the visible wavelength, a drastic decrease in the optical transmittance at the onset of the ultraviolet wavelength (~370 nm) due to the film's absorption originating from the energy bandgap can be seen. As a 10 nm thick Cu layer deposited onto the TiO_x film, an apparent reduction in the optical transmittance and redshift of the absorption edge was observed. The opaque nature of the Cu metal led to the average transmittance around the visible wavelength decreasing to about 60%. For the TiO_x/Cu structure treated by the RTA process, the average transmittance around the visible wavelengths was somewhat higher than that of the as-deposited TiO_x/Cu structure, while the absorption edge at the UV wavelength of these annealed samples was almost the same as the as-deposited one. This result reveals that the thin metallic Cu and the oxidized Cu layer covered on the TiO_x film both showed a similar obstruct feature as at the visible light, it also occurred in the marked redshift of the absorption edge when compared with that of the single TiO_x film.

Figure 2a–e respectively show the surface morphologies of the TiO_x film and the TiO_x/Cu structures before and after processing the RTA treatment at temperatures of 250 °C, 350 °C, and 450 °C (the cross-sectional images of the as-deposited and 250 °C-annealed TiO_x/Cu structure are also shown in the inset figures). The surface of the anatase–TiO_x film

(Figure 2a) was uneven, with irregular grains and visible boundaries. Those fine grains distributed over the TiO_x surface became invisible as the film was covered by a 10 nm thick Cu layer (Figure 2b). The grain boundaries distributed over the surface were then hardly evident, resulting in an ambiguous surface morphology as the TiO_x/Cu structure annealed at 250 °C (Figure 2c). The surface morphology of the 350 °C-annealed TiO_x/Cu structure (Figure 2d) became more ambiguous with the appearances of voids and white protrusions. When the annealed temperature reached 450 °C, as shown in Figure 2e, the voids that might be relevant to the outdiffusion of the oxidized Cu layer were comprehensively distributed over the structural surface. Moreover, although the layered structure could be roughly defined from the inset figures, the change in the microstructures at the TiO_x/Cu interface affected by the annealing process was hardly observed.

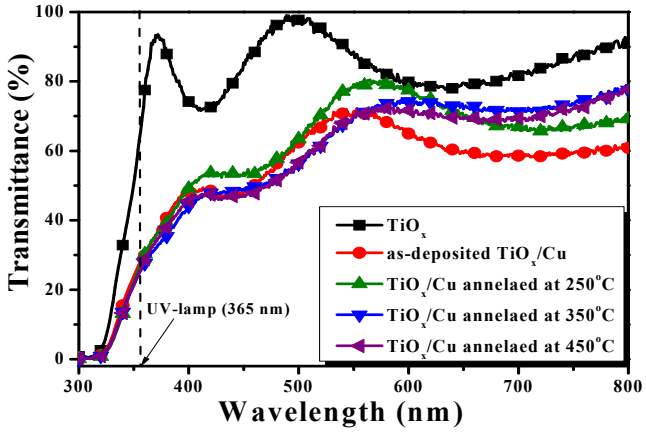

Figure 1. Optical transmittance of a 10 nm thick Cu layer deposited onto the TiO_x film and sequentially treated by an RTA process at temperatures of 250 °C, 350 °C, and 450 °C for 1 min under ambient oxygen, as well as the single TiO_x film.

The crystallinity of the as-deposited and annealed TiO_x/Cu structures, as well as the single TiO_x film conducted from the XRD measurements, are presented in Figure 3. The TiO_x film formed the polycrystal structure with only the anatase phase of the two apparent crystal planes, (hkl), of (101) and (112) and a weak plane of (200) (the diffraction peaks for the anatase phase are taken from the JCPDS No.021-1272 and are marked as "A," with the crystal plane (hkl) also given). As thin Cu layers coated onto the TiO_x film, the diffraction peaks and their positions associated with different crystal planes of the anatase structure in the XRD spectrum were basically identical to the single TiO_x film. For the TiO_x/Cu structures annealed at temperatures of 250 °C, 350 °C, and 450 °C, the resulting respective XRD patterns still exhibited the anatase phase with dominant crystal planes of (101) and (112). The intensity and position of these two crystal planes were almost identical to that of the single TiO_x film. This result reveals that neither the metallic Cu deposition nor the following oxidation process on the TiO_x/Cu structure affected the crystallinity of the under-layered TiO_x film. Moreover, no clear evidence of the Cu atoms being doped into the TiO_x matrix emerged, as the peak positions of the two anatase planes that appeared in the XRD spectra were basically duplicates of the single TiO_x film. In addition to the investigations on the crystallinity of the under-layered TiO_x film, no featured peaks related to the upper-layered Cu could be identified from these XRD spectra. This might be because the signal related to the metallic Cu and/or its oxidized states was too weak to be observed by the XRD measurements. Accordingly, further observation on the changes of the metallic Cu layer oxidized by the annealing process was essential.

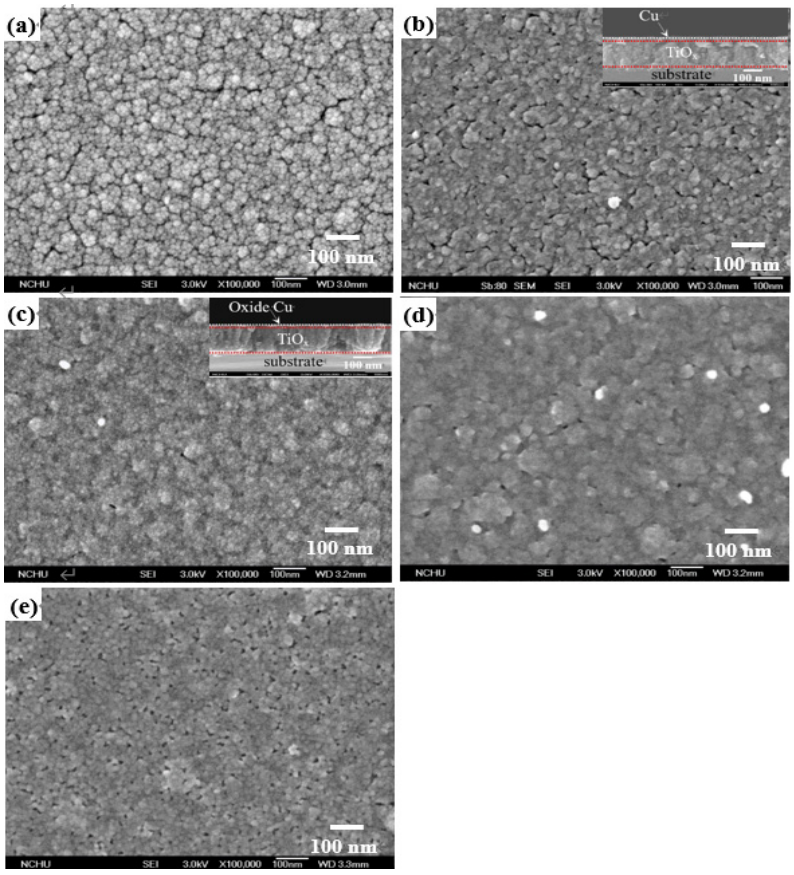

Figure 2. Surface morphologies of the (**a**) TiO_X film and the (**b**) as-deposited TiO_X/Cu structure, and the TiO_X/Cu structures annealed at temperatures of (**c**) 250 °C, (**d**) 350 °C, and (**e**) 450 °C (the cross-sectional images of the as-deposited and 250 °C-annealed samples are also shown in the inset figures).

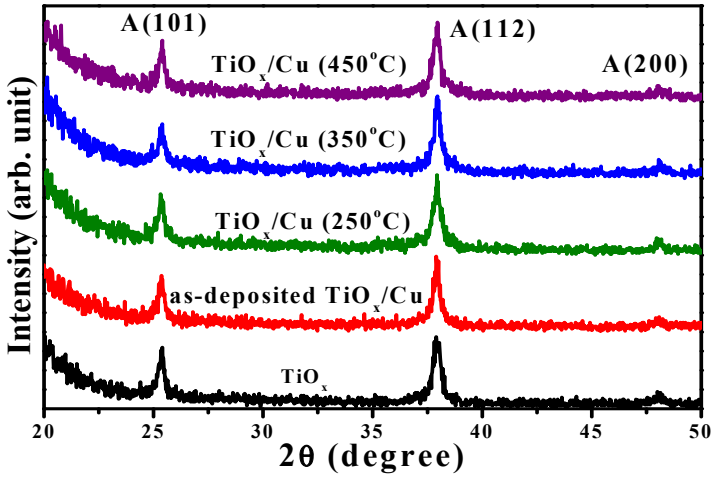

Figure 3. X-ray diffraction spectra of the single TiO_X film, the as-deposited TiO_X/Cu structure, and the TiO_X/Cu structures annealed at temperatures of 250 °C, 350 °C, and 450 °C (the diffraction peaks for the anatase phase are marked as "A," with the crystal planes (hkl)).

Figure 4 represents the degradation rate associated with the concentration evolution on the MB solution as a function of the UV light irradiation time catalyzed using the single Cu and TiO_X films as well as the as-deposited and annealed TiO_X/Cu structures (the change in the concentration of the MB solution directly irradiated by the UV light is also given as a comparison). According to the limited degradation rate in the MB concentration, as the irradiation time increased, both the MB solution itself and the solution catalyzed by

the single 200 nm thick Cu film were only slightly reactive to the UV light illumination. In contrast, the MB solution decomposed by the UV light irradiation, together with the TiO_x film catalyzation, was significantly enhanced, as could be seen in the marked reduction in the concentration rate as the irradiation time increased. As a thin Cu layer covered the TiO_x film, the resulting decomposition efficiency catalyzed by this TiO_x/Cu structure became apparently inferior to the TiO_x film, even when this structure annealed at a temperature of 250 °C. In contrast to the as-deposited and 250 °C-annealed TiO_x/Cu structures, the UV light-induced decomposition to the MB solution incorporating the 350 °C-annealed TiO_x/Cu structure was greatly enhanced, which demonstrates that the degradation rate was clearly faster than that of the MB solution photo-catalyzed only by the TiO_x film. The resulting degradation rate of the MB solution catalyzed using the TiO_x/Cu structure after being annealed at an elevated temperature of 450 °C was again not as good as the degradation rate using the single TiO_x film. The rate constant, k, which is derived by fitting the concentration evolution of the MB solution under UV light irradiation, complied with the first-order rate equation, which is addressed as the following equation that was employed to quantify the decomposition ability of the MB solution [28]:

$$\ln\left(\frac{C}{C_0}\right) = kt \quad (1)$$

where C and C_o are the concentrations of the MB solution under UV light irradiation times of $t = 0$ and t, respectively. The rate constant values analyzed from the curves in Figure 4 are summarized in Table 1. The decomposition of the MB solution catalyzed by the Cu film under UV light irradiation corresponded to a rate constant (~0.0038 min^{-1}) similar to the value derived from the MB solution directly decomposed by UV light illumination (~0.0036 min^{-1}). This decomposition increased markedly to about 0.0120 min^{-1} as the solution was photo-decomposed by incorporating the single TiO_x film. The value decreased to about 0.0091 min^{-1} as the solution catalyzed when using the TiO_x film covered by a 10 nm thick Cu layer, and a low value of about 0.0087 min^{-1} was derived from the degradation rate of the MB solution using the 250 °C-annealed TiO_x/Cu structure. When the TiO_x/Cu structure was annealed at a temperature of 350 °C, the specimen used to photo-decompose the MB solution corresponded to the highest rate constant of about 0.0165 min^{-1}. It then decreased to about 0.0118 min^{-1}, as derived from the MB solution photo-decomposed by using the TiO_x/Cu structure annealed at an elevated temperature of 450 °C. This result indicates that the UV-activated degradation rate of the MB solution could be enhanced by more than three times as it was photo-catalyzed using the single TiO_x film. The degradation efficiency of the MB solution could be further improved by about 40% with the assistance of an oxidized Cu layer annealed at 350 °C, while other annealed treatments on the Cu layer showed little support or even obstructed the TiO_x film's ability to photo-decompose the MB solution.

Table 1. Rate constant (k) and reduction percentage (R) of the TiO_x film, and the as-deposited and annealed TiO_x/Cu structures to decompose the MB solution and sterilize the *E. coli* under UV light irradiation.

	Cu	**TiO_x**	**As-Deposited**	**250 °C**	**350 °C**	**450 °C**
k (min^{-1})	0.0038	0.0120	0.0091	0.0087	0.0165	0.0118
R (%)	37	64	54	43	91	68

k value of MB solution is 0.0036 min^{-1}.

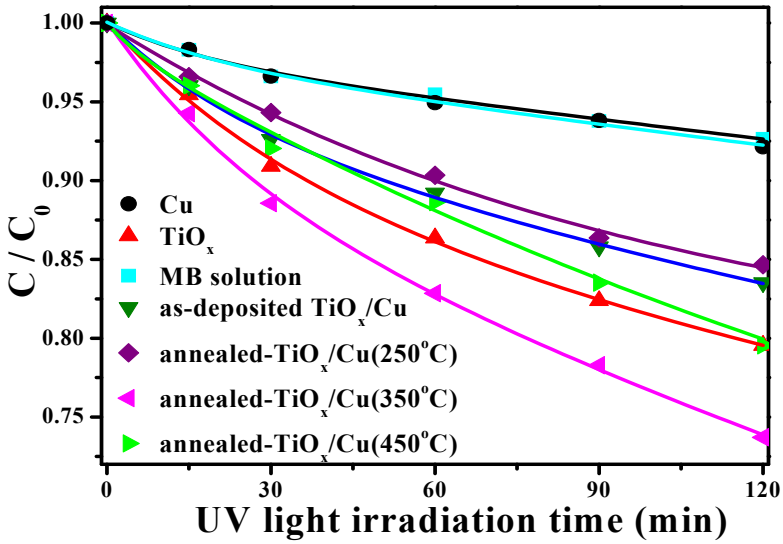

Figure 4. Concentration evolution of the MB solution as a function of UV light irradiation time catalyzed using the single Cu and TiO_x films, and the as-deposited and annealed TiO_x/Cu structures (the change on the concentration of the MB solution directly irradiated by the UV light is also given as a comparison).

Figure 5a–d respectively show the photographs of the *E. coli* bacterial colonies on the nutrient agar after a 24 h incubation period, sterilized using the UV light-activated as-deposited and annealed TiO_x/Cu structures. The photographs of the plate for the *E. coli* bacterial colonies that were directly illuminated by the UV light (Figure 5e, the *E. coli* bacterial colonies sterilized using the single Cu (Figure 5f) and TiO_x (Figure 5g) films are also given as a comparison). Although the UV-activated Cu film was inactive while decomposing the MB solution, it showed the functional ability to inhibit the growth of the *E. coli* bacteria. The number of bacterial colonies counted from the plate (Figure 5f) decreased to about $(87 \pm 5.2) \times 10^3$ CFU/mL, whereas the *E. coli* bacteria directly illuminated by the UV light irradiation was about $(138 \pm 5.5) \times 10^3$ CFU/mL (Figure 5e). The growth of the *E. coli* bacteria could be further controlled to about $(50 \pm 4.9) \times 10^3$ CFU/mL while the Cu film was substituted by the TiO_x film (Figure 5g). These results indicate that the UV-activated Cu and TiO_x films are both beneficial for suppressing the growth of *E. coli* bacteria. When a thin copper layer was coated onto the TiO_x film, the resulting bacterial colonies appearing on the plate, as shown in Figure 5a, were about $(64 \pm 4.9) \times 10^3$ CFU/mL. Although this value is somewhat higher than that of the bacterial colonies using the single TiO_x film, the suppressed efficiency in the growth of the *E. coli* bacteria is still apparent when compared with the sterilization using only the single Cu film. Thus, it can be concluded that the under-layered TiO_x film in the TiO_x/Cu structure also played an important part in inhibiting the growth of the *E. coli* bacteria. As the TiO_x/Cu structure annealed at a temperature of 250 °C, the growth of the bacterial colonies that appear in Figure 5b was slightly increased to about $(79 \pm 5.0) \times 10^3$ CFU/mL). By contrast, the growth of the bacterial colonies could be minimized to about $(12 \pm 2.1) \times 10^3$ CFU/mL, as the *E. coli* bacteria were sterilized using the 350 °C-annealed TiO_x/Cu structure (Figure 5c). An increase in the number of bacterial colonies (~$(45 \pm 3.5) \times 10^3$ CFU/mL) was observed from the plate sterilized using the 450 °C-annealed TiO_x/Cu structure (Figure 5d). The reduction percentage, *R*, which quantitatively represents the antibacterial activity of the specimen under UV lamp irradiation, is determined by the evolution of the bacterial colonies on the plate using the following equation [29]:

$$R\ (\%) = [(A - B)/A] \times 100\% \quad (2)$$

where *A* is the number of the bacterial colonies counted from the *E. coli* directly sterilized by the UV lamp irradiation and *B* is the number of the bacterial colonies counted from the plate treated by the specimen incorporation. The higher the reduction percentage, the better the antibacterial activity. Table 1 summarizes the reduction percentages of the plates shown in Figure 5. According to this table, the antibacterial activity of the single TiO_x film (~64%) was almost twice as high as the single Cu film (~37%). The degree for the antibacterial activity of the TiO_x film decreased somewhat to about 54% as a semi-opaque Cu layer covered the TiO_x film. The structural activity to sterilize the *E. coli* bacterial was continuously deteriorated (~43%) as it was annealed at a temperature of 250 °C. In contrast to the 250 °C-annealed sample, a remarkable increase in antibacterial activity (~91%) was obtained from the TiO_x/Cu structure annealed at a temperature of 350 °C. The antibacterial activity was again decreased to about 68% while the annealed temperature on the TiO_x/Cu structure reached 450 °C. According to the values listed in Table 1, although the degrees of the rate constant and reduction percentage using the single Cu film were both inferior to those when using the single TiO_x film, the photocatalytic and antibacterial activities for the Cu coated onto the TiO_x film could still be optimized as this structure annealed at a temperature of 350 °C.

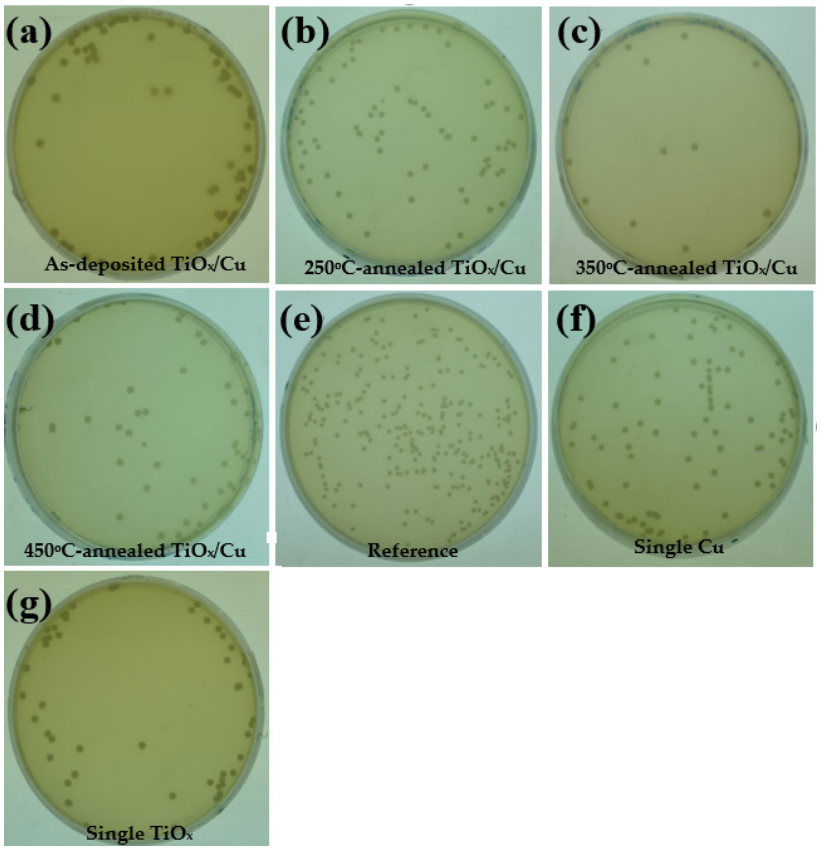

Figure 5. Photographs of the *E. coli* bacterial colonies on the nutrient agar after a 24 h incubation period, sterilized using the (**a**) as-deposited, (**b**) 250 °C-, (**c**) 350 °C-, and (**d**) 450 °C-annealed TiO_x/Cu UV light-activated structures, respectively (images of the *E. coli* bacterial colonies directly illuminated by the UV light (**e**) (reference) as well as the *E. coli* bacterial colonies that were sterilized and incorporated with the single Cu (**f**) and TiO_x (**g**) films are also given as a comparison).

Figure 6 depicts the rate constant and reduction percentage of the as-deposited and annealed TiO_x/Cu contact systems as well as the single Cu and TiO_x films listed in Table 1. The inactive behavior of the single Cu layer and the good photocatalytic activity of the anatase–TiO_x film under UV light irradiation resulted from the formation of the surface

hydroxyl radicals that could be clearly seen from the significant difference in the values of their rate constants. However, though the Cu layer was inactive to the UV light irradiation, the metallic Cu showed an ability to inhibit the growth of the *E. coli* as a consequence of the bacterial cell being broken by the Cu ion and this ability corresponded to a reduction percentage of 37%. When a thin Cu layer is coated onto the TiO_x film, this structure becomes activable by the UV light irradiation, as observed in the comparison of its rate constant to that of the single Cu layer. However, the shielding effect of the UV light by the surface Cu layer results in an inferior rate constant than the single TiO_x layer. In contrast, the photocatalytic activity induced by the under-layered TiO_x film was found to be beneficial for enhancing the structural antibacterial ability to a value of 54% as compared with that of the single Cu layer. It can also be seen that there was only little change in the rate constant from the 250 °C-annealed TiO_x/Cu structure, while an obvious decrease in the reduction percentage was derived. This reveals that the UV-activated property of this structure was nearly changed, but that the amount of the Cu ions required to break the bacteria had been significantly reduced as a consequence of the oxidation treatment. Both the rate constant and reduction percentage were optimized as the TiO_x/Cu structure was annealed at 350 °C, and these values decreased again when the structure was annealed at a temperature of 450 °C. This suggests that a different mechanism dominated the increase in the photocatalytic activities of these annealed TiO_x/Cu contact systems. As there was neither a change in the crystallinity nor evidence of a new compound or dopant formation in the TiO_x film, the ability of the annealing process on the oxidation of the upper-layered Cu to affect the TiO_x/Cu contact interface might be crucial for determining the structural activities required to decompose the MB solution as well as sterilize the *E. coli* bacterial.

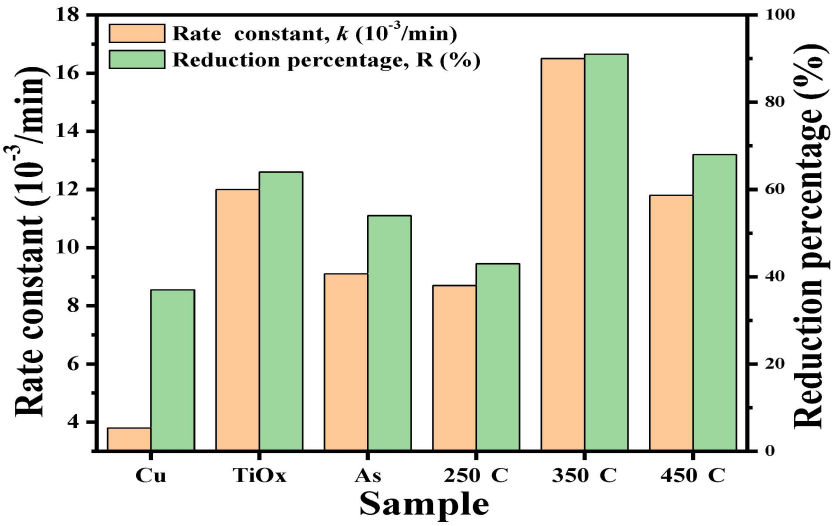

Figure 6. Rate constant and reduction percentage of the as-deposited and annealed TiO_x/Cu contact systems as well as the single Cu and TiO_x films.

With the aim of investigating the annealing process on the changes of the chemical bond configurations, the compositions for the Ti, Cu, and O elements at the contact interface of these TiO_x/Cu structures were examined using XPS measurements through Ar^+ sputtering etching. Figure 7a–c respectively show the spectra of the binding energies related to the Ti 2p, Cu 2p, and O 1s core levels at the interface of the TiO_x/Cu structure after etching by the Ar^+ sputtering for 60 s. The intensity of the binding energy scales was normalized according to the maximum value in the corresponding XPS spectrum. The Ti $2p_{3/2}$ and Ti $2p_{1/2}$ signal at binding energies of 458.2 and 464.0 eV, respectively, with a difference of 5.8 eV, were measured from the interface of the as-deposited TiO_x/Cu contact system (Figure 7a). The binding energies and their difference are consistence with the reports on

the TiO_2 film with anatase structure, which could be denoted as the bond configuration of Ti(IV) in the spectrum [1,30–35]. When the contact system annealed at a temperature of 250 °C, the Ti $2p_{3/2}$ signal shifted slightly to a lower binding energy of 458.0 eV, with a narrow difference between the signal of the Ti $2p_{3/2}$ and Ti $2p_{1/2}$ (~5.5 eV). This signal shifted clearly to 457.4 eV as the contact system annealed at 450 °C. As quoted from the bond configurations of the Ti species, the shift of the binding energy was ascribed to the appearance of the Ti(III) bond originating from the formation of the oxygen vacancies in the TiO_x film [5,36,37]. It also addresses how the higher the amount of oxygen vacancies that are distributed over the TiO_x film the lower the position of the binding energy of the Ti $2p_{3/2}$ signal. Based on the changes in the binding energy of the Ti $2p_{3/2}$ signal, it could be inferred that the oxygen vacancies distributed over the surface of the TiO_x film gradually increased as the annealing temperature on the structure increased. In the Cu 2p spectra (Figure 7b), two feature peaks emerged from the Cu $2p_{3/2}$ and Cu $2p_{1/2}$ spin-orbits, with almost the same difference in the binding energy (~19.8 eV), something which could be measured from all of the samples. The binding energy of the Cu $2p_{3/2}$ signal (~932.8 eV) obtained from the as-deposited TiO_x/Cu structure was consistent with the signal measured from the metallic and/or low oxidized Cu states (denoted as Cu(0)/Cu(I) in the spectra) [38–42]. As the annealing temperature on this contact system increased, this signal gradually shifted toward a higher binding. The shift of the binding energy is related to the increase in the highly oxidized Cu state (denoted as Cu(II) at about 934.5 eV in this figure), which appeared at the interface of the TiO_x/Cu structure [40–44]. This implies that the oxidization of the element Cu in the TiO_x/Cu contact system after the annealing treatment can be traced with XPS analysis, though these Cu-oxidized states were little observed from their corresponding XRD patterns. In addition, the composition of these oxidized Cu states at the TiO_x/Cu contact system could also be estimated by deconvoluting the Cu $2p_{3/2}$ signal into the overlapping peaks related to the Cu (II) and Cu(0)/Cu(I) states. According to the deconvolved area of the Cu(II) and Cu(0)/Cu(I) states, the composition of the highly oxidized state (Cu(II)) at the TiO_x/Cu interface rose from 0.31 to 0.47 and then to 0.71 as the contact structure's annealing temperature increased from 250 °C to 450 °C. The O 1s signal measured from the interface of the as-deposited TiO_x/Cu structure (Figure 7c) at about 529.7 eV was correlated to the O-Ti(IV) chemical bond [5,32]. As the annealing treatment on the TiO_x/Cu contact system, the O 1s signal became very significant (the original signal is about twice that of the as-deposited sample), revealing that a large number of the Cu atoms had been oxidized and come to dominate the spectra. The binding energies of the O 1s signal shifted from 529.9 eV to 530.1 eV as the annealing temperatures on the TiO_x/Cu structure increased from 250 C to 350 °C. In reference to the reports on the oxidized states of the Cu element, the increase in the formation of the O-Cu(I) chemical bond (~530.4 eV) at the interface of the TiO_x/Cu contact system was responsible for the shift of the binding energy [34,41,45]. It is worth noting that the O 1s signal clearly shifted to a low binding energy of about 529.8 eV as the contact system annealed at a temperature of 450 °C. This result implies that such an annealing treatment would cause the O-Cu(I) oxidized state to evolve into the highly oxidized state that was related to the O-Cu(II) chemical bond (denoted at a binding energy of 529.7 eV in the spectra) [38,45]. Incorporating the analysis on the Cu 2p and O 1s core levels, it can be seen that the Cu(0) state's contact with the TiO_x film predominated over the interface of the as-deposited TiO_x/Cu structure, while this contact gradually evolved into a TiO_x/O-Cu(I) feature as the heterojunction structure oxidation occurred at 250 °C. As the annealed temperature reached 350 °C, more O-Cu(I) states were in contact with the TiO_x film. Eventually, the O-Cu(II) state became the dominant bonding type at the interface of the 450 °C-annealed TiO_x/Cu structure. Based on the investigations of the chemical bond configurations at the interface of these TiO_x/Cu

structures, it was confirmed that the nanocomposite TiO_x/Cu_xO heterojunction structure could be realized simply by the annealing treatment. The amount of the Cu element in a highly oxidized state increased with the annealing temperature, while that of the Ti element in the surface of the TiO_x film evolved from a Ti(IV) to a Ti(III) state, revealing that the annealing process not only resulted in the oxidation of the Cu atoms but also caused the outdiffusion of the oxygen atoms from the TiO_x film into the Cu layer. As quoted from the reports, the photo-induced EHP from the Ti(III) oxidized state has also been demonstrated to be separated more effectively than that from the Ti(IV) oxidized state to result in a better photocatalytic activity [5,17].

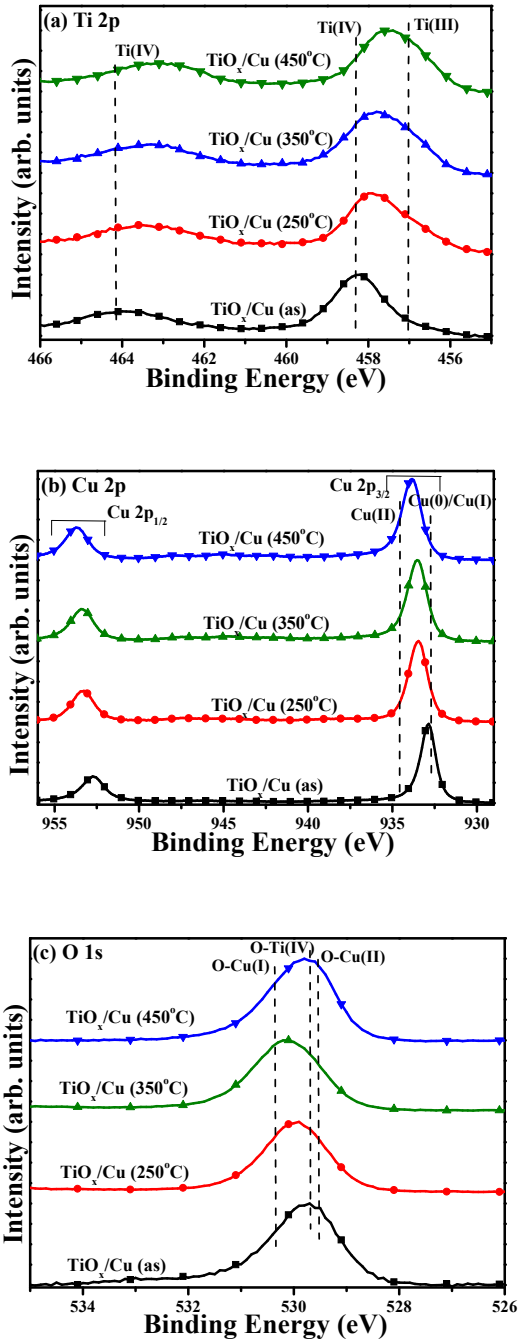

Figure 7. Binding energy spectra of the (**a**) Ti 2p, (**b**) Cu 2p, and (**c**) O 1s core levels measured from the surface of the as-deposited TiO_x/Cu structure and the TiO_x/Cu structures annealed at temperatures of 250 °C, 350 °C, 450 °C, respectively.

In order to further investigation the crystalline evolution of the single Cu layer affected by the annealing process, 200 nm thick Cu films were directly deposited onto the silicon substrate and processed at annealing temperatures of 250 °C, 350 °C, and 450 °C. Figure 8 depicts the crystalline evolutions of the as-deposited and annealed Cu films conducted by XRD measurement. The diffraction spectrum of the as-deposited Cu film exhibited only two dominant peaks at about 43.42° and 50.58°, respectively. These peaks could be identified as the face-centered cubic (fcc) structure of the crystal planes (hkl) of (111) and (200) (JCPDS No. 003-1018). As the Cu film annealed at a temperature of 250 °C under ambient oxygen, this thermal oxidation process resulted in another broad peak at about 36.06° other than the crystal planes correspondent with the metallic Cu structure in the XRD spectrum. According to the JCPDS No. 005-0667, this broad peak could be denoted as the oxidized structure of the cuprous oxide phase with the crystal plane (hkl) of (111). This transitionally oxidized Cu phase has also been reported to occur due to the insufficient activation energy between the copper and oxygen atoms [24,46,47]. The Cu_2O(111) crystal plane became the dominant diffraction signal, while those of the crystal planes related to the metallic Cu (Cu(111) and Cu(200)) were absent in the XRD spectrum, as the single Cu film was annealed at 350 °C. In addition, a broad and weak diffraction peak at about 38.66°, identified as the crystal plane belonging to the cupric oxide crystalline phase (denoted as the crystal plane (hkl) of (200), per JCPDS No. 041-0254), also appeared in the XRD spectrum. As referred to in previous reports, the formation of this highly oxidized state of copper was correlated with the adequate thermal activation of copper and oxygen atoms [46,48]. This cupric oxide phase, with specific peaks correspondent to the crystal plane (hkl) of (211) and (200), then predominated over the XRD spectrum when the Cu film was annealed at 450 °C. According to the crystalline evolution of the thermally oxidized Cu layer and the chemical bonds of the oxidized Cu states at the interface of the annealed TiO_x/Cu structures, it can be concluded that the metallic copper film was oxidized as the intermediate Cu_2O phase while it was annealed at a low temperature and that the stable CuO phase formed as the metallic Cu layer annealed at an elevated temperature. The results are consistent with previous studies which demonstrate that the appearance of the phases for the oxidized Cu structure is closely related to the annealing temperature and ambient oxygen [22,48].

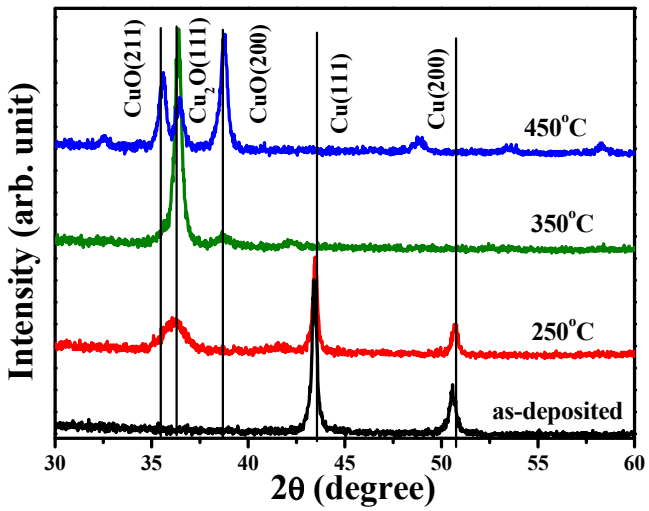

Figure 8. Crystalline evolutions of the as-deposited 200 nm Cu film and the films annealed at 250 °C, 350 °C, and 450 °C, conducted by XRD measurement (the correspondent crystal planes (hkl) are also given).

The electrical properties of the single Cu film oxidized at temperatures of 250 °C, 350 °C, and 450 °C are summarized in Table 2. The as-deposited Cu film possessed high

electron carriers of about 2.49 × 10^{22} cm^{-3}, with the mobility of 162 cm^2/V s. A small decrease in electron carriers (~2.07 × 10^{22} cm^{-3}) was measured as the Cu film oxidized at a temperature of 250 °C, which could be attributed to the intermediate Cu_2O phase that was formed in the metallic Cu matrix. The conductive type, converted into *p*-type conduction with the hole carriers of about 6.03 × 10^{16} cm^{-3}, was obtained as the Cu film was oxidized at an annealing temperature of 350 °C. This change in the conductive type could be connected to the metallic Cu being completely transformed into the oxidized Cu_2O phase with the limited formation of the CuO phase, both of which have been demonstrated to be *p*-type semiconductors [23,24,47,49,50]. The structure that developed a composition of Cu_2O and CuO phases as the Cu film oxidized at 450 °C also showed *p*-type conduction, with a similar hole concentration of about 3.66 × 10^{16} cm^{-3}. The investigation on the crystalline structure of the oxidized Cu layer suggests that the TiO_x/Cu contact system evolved into the TiO_x/(Cu + Cu_2O) contact system after being annealed at 250 °C under ambient oxygen. A completely oxidized structure constructed from the Cu_2O phase with a little of the CuO phase was subsequently formed and contacted the TiO_x film when the annealed temperature on the structure reached 350 °C. Eventually, the oxidized CuO phase became the dominant structure contacted to the TiO_x film as the contact system annealed at a temperature of 450 °C. Although the conductivity of the anatase–TiO_x film prepared in this study was too low to be measured, it should demonstrate the *n*-type conductivity that is associated with the dominated oxygen-vacancy defects in the film [18,51,52]. Accordingly, it could be considered that the as-deposited and 250 °C-annealed TiO_x/Cu contact systems formed a homogeneous heterojunction in *n*-type conduction. On the contrary, as *p*-type conductivity was measured from the single Cu film annealed at 350 and 450 °C, it can be suggested that the heterojunction structures with the opposite conductivity type (eq. *n*-TiO_x/*p*-Cu_xO) are formed as the TiO_x/Cu contact system annealed at these two temperatures. Accordingly, an extra electrical field was built at the interfaces of the 350 °C- and 450 °C-annealed TiO_x/Cu structures, which was beneficial for separating the EHPs generated at the contact interface under UV light irradiation. The products of the hydroxyl (·OH) and superoxide anion ($\cdot O_2^-$) radicals originating from the electron and hole carriers, respectively, reacted with the ambient vapor and oxygen and thus could be enhanced due to the inhibition of the recombination of the photo-generated EHPs. As these ·OH and $\cdot O_2^-$ radicals form the primary functional group for catalyzing the decomposition of the organic compounds and for breaking the membrane of the bacteria on the TiO_x surface [53–56], the resulting 350 °C- and 450 °C-annealed TiO_x/Cu contact systems that behaved as the *n*/*p* heterojunction structure therefore demonstrated superior activity in decomposing the MB solution and sterilizing the *E. coli*, as listed in Table 1 and Figure 6.

Table 2. Electrical properties as a function of the 200 nm Cu film annealed at various temperatures under ambient oxygen for 1 min.

	Conc. (cm^{-3})	**μ_n (cm^2/V s)**	**ρ (Ω cm)**
As-deposited	−2.49 × 10^{22}	1.62 × 10^2	1.55 × 10^{-6}
250 °C	−2.07 × 10^{22}	1.54 × 10^2	1.96 × 10^{-6}
350 °C	6.03 × 10^{16}	1.56	6.63 × 10^1
450 °C	3.66 × 10^{16}	2.67	6.39 × 10^1

Except for the built-in voltage established at the interface of the 350 °C- and 450 °C-annealed TiO_x/Cu structure for separating the photo-generated EHPs, the band offset between the anatase–TiO_x and the oxidized Cu states should also be noted, as it was crucial for driving the migration of these photo-generated carriers. The band offset between two materials is established from the discontinuity of the conduction (ΔE_c) and valence (ΔE_v) bands origi-

nating from the differences in the material's energy bandgap (E_g) and electron affinities ($q\chi$). As quoted from [23,24,49,57], *p*-type Cu_2O and CuO possess the energy bandgaps of about 2.2 eV and 1.7 eV, respectively, with electron affinities of about 3.3 eV and 3.8 eV. Incorporating the energy bandgap (~3.2 eV) and electron affinity (~3.9 eV) of the anatase–TiO_2 phase, the conduction and valence band offsets between the TiO_2 and Cu_2O were 0.6 and 1.6 eV, respectively, while those of the band offsets between the TiO_2 and CuO were 0.1 and 1.6 eV. Thus, the conduction band of the *p*-type Cu_2O was more negative than that of the *n*-type TiO_2, whereas the band offset of the conduction band between the *p*-type CuO and *n*-type TiO_2 was relatively invisible. In contrast to the remarked difference in the band offset of the conduction band, the valence band of both the *p*-type Cu_2O and CuO possessed almost the same anodic potential, which was less than that of the TiO_2. This result suggests that the electron carriers at the *n*-TiO_x/*p*-Cu_2O interface in this study, generated under UV light irradiation, would be more prone to migrate to the TiO_x side than that of the carriers generated at the *n*-TiO_x/*p*-CuO contact system, while a similar driving force appeared to cause the photo-generated hole carriers from the *n*-type TiO_x side to the *p*-type Cu_2O or CuO interfaces. Thus, the recombination of the EHPs generated under UV light irradiation at the *n*-TiO_x/*p*-Cu_2O interface would be inhibited more effectively as a result of the *n*-TiO_x/*p*-Cu_2O structure possessing a superior band offset discontinuity than that of the *n*-TiO_x/*p*-CuO structure.

Figure 9 shows three cycles for the response of the photo-excited current as functions of the transient of the 350 °C- and 450 °C-annealed TiO_x/Cu structures as well as the on–off current transient measured from the single TiO_x film. The photo-induced currents of these samples under UV light irradiation are reproducible and reliable, as could be seen from the three cycles' on–off current transient. The single TiO_x film and the 350 °C- and 450 °C-annealed TiO_x/Cu structures possessed dark currents of about 9.64×10^{-9} A, 2.05×10^{-8} A and 1.90×10^{-8} A, respectively. As the TiO_x film was illuminated by the UV light, the photo-generated carriers increased the current to about 8.62×10^{-7} A. In contrast to the TiO_x film, a large photo-excited current of approximately 1.96×10^{-5} A was measured from the 350 °C-annealed TiO_x/Cu sample after being irradiated by the UV light. As the TiO_x/Cu structure was annealed at 450 °C, a photo-induced current of about 2.16×10^{-6} A was measured. Incorporating the changes in currents of these structures before and after the UV light illumination, the on–off current transient (i.e., the ratio of the photo-excited current to the dark current) of the 450 °C-annealed TiO_x/Cu structure (~113) was somewhat higher than that of the TiO_x film (~89), whereas an apparent increase could be obtained from the on–off current transient of the 350 °C-annealed TiO_x/Cu structure (~953). Based on the above-mentioned investigation, the reason for the increase in the on–off current transient for those two annealed TiO_x/Cu structures was the formation of the *n/p* heterojunction, which was helpful for the separation of the photo-generated carriers. Moreover, the way in which the 350 °C-annealed TiO_x/Cu structure possesses a dominant *n*-TiO_x/*p*-Cu_2O interface with significant band offsets between the conduction and valence bands' discontinuity could be a critical reason for the corresponding order of magnification that we find on the photo-induced current when compared with the 450 °C-annealed sample. This sample also demonstrated a longer transient time, as determined from the highest photo-excited current to the dark current (7 min), when compared with that of the 450 °C-annealed sample (4 min). Accordingly, the *n*-TiO_x/*p*-Cu_2O heterojunction predominated over the 350 °C-annealed TiO_x/Cu structure, which significantly enhanced the photo-excited carriers and resulted in a longer carrier lifetime, exhibiting the quality behavior required to decompose the MB solution and inhibit *E. coli* growth under UV light irradiation. Based on the mechanism established from this study, the *p*-type conduction abundant in the Cu(I) oxidized state

(ie. Cu_2O crystalline structure) is essential for improving the photocatalytic activity of the TiO_x/Cu contact system.

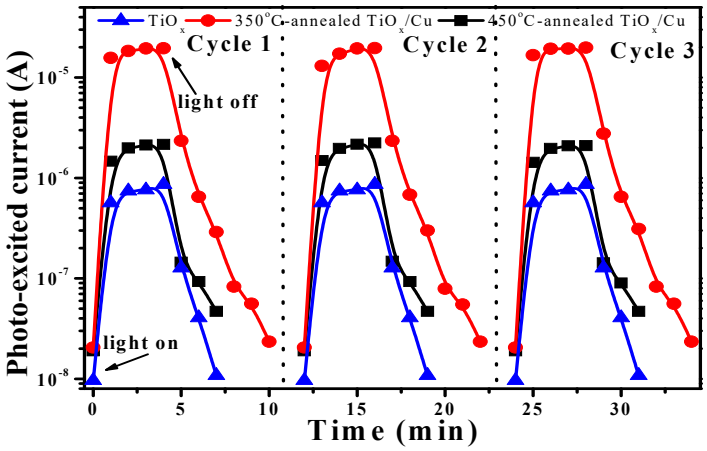

Figure 9. On–off current transient of the 350 °C- and 450 °C-annealed TiO_x/Cu structures as well as the single TiO_x film irradiated by the UV lamp.

4. Conclusions

In this work, an oxidized TiO_x/Cu structure was prepared simply by a thermal annealing process under ambient oxygen. Compared with the optical spectra of a single TiO_x film, both the as-deposited and annealed TiO_x/Cu structures showed a reduction of about 20% for the optical transmittance within the visible wavelengths and a redshift of the absorption edge at the early UV wavelength. In addition, no compound related to the Ti-Cu alloys and also no trace of the Cu doping into the TiO_x matrix could be found from these TiO_x/Cu contact systems. Although the optics and crystallinity of these annealed TiO_x/Cu structures were almost similar to those of the as-deposited structure, their photocatalytic activities for decomposing the MB solution and inhibiting the growth of the *E. coli*. bacteria showed variation with the annealed temperatures. With the help of the studies on the chemical bond configurations at the interface of the TiO_x/Cu structures as well the crystalline and electrical evolution of the single Cu layer under the same annealing temperatures, the photocatalytic activity of these TiO_x/Cu contact systems was found to be deeply correlated to the changes of the oxidation states and conduction types of the upper-layered Cu. The type-conversion of the oxidized Cu layer at the annealed temperatures of 350 °C and 450 °C realized the formation of the nanocomposite *n*-TiO_x/*p*-Cu_xO heterojunction structures. Such a hetero-contact system was beneficial for the separation of the photogenerated EHPs over the TiO_x surface. Moreover, since the band offset between the *n*-TiO_x/*p*-Cu_2O structure was more significant than that of the *n*-TiO_x/*p*-Cu_2O structure, the *p*-type Cu_2O crystalline phase that predominated over the 350 °C-annealed TiO_x/Cu system results in the better separation of the photo-generated EHPs than that of the 450 °C-annealed sample, at which temperature most of the Cu_2O structures had evolved into the CuO structures. The photocatalytic activity of the TiO_x film could further be optimized as the surface modified by a thin Cu layer and then oxidized at a temperature of 350 °C. The rate constant of the 350 °C-annealed TiO_x/Cu structure derived from it decompose the MB solution under UV light irradiation was 38% higher than that of the single TiO_x film. Furthermore, this structure irradiated by the UV lamp for 1 h almost completely inhibited the growth of the *E. coli* bacteria for 24 h (the reduction percentage was about ~91%).

Author Contributions: D.-S.L. organized and designed the experiment procedures; J.-A.C. and S.-M.T. supported the measurement apparatus and wrote this paper; Y.-Y.H. executed the film deposition; P.-J.S. performed and supported the thin film measurements and analysis. All authors have read and agreed to the published version of the manuscript.

Funding: This research was funded by Ministry of Science and Technology under MOST 109-2622-E-150-023.

Institutional Review Board Statement: Not applicable.

Informed Consent Statement: Not applicable.

Data Availability Statement: The original contributions presented in this study are included in the article. Further inquiries can be directed to the corresponding author.

Acknowledgments: The authors also would like to acknowledge the support by ITRI and MIRDC.

Conflicts of Interest: The authors declare that there are no conflicts of interest regarding the publication of this paper.

References

1. Huang, J.J.; Lin, C.C.; Wuu, D.S. Antireflection and passivation property of titanium oxide thin film on silicon nanowire by liquid phase deposition. *Surf. Coat. Technol.* **2017**, *320*, 252–258. [CrossRef]
2. Omprakash, S.S.; Naveen Kumar, S.K.; Ravishankar, H. Titanium dioxide and zinc oxide as a dielectric material for application in TFT's. *Mater. Today* **2018**, *5*, 10833–10838. [CrossRef]
3. Holland, A.; McKerracher, R.; Cruden, A.; Wills, R. Electrochemically treated TiO_2 for enhanced performance in aqueous Al-ion batteries. *Materials* **2018**, *11*, 2090. [CrossRef] [PubMed]
4. Mamaghani, A.H.; Haghighat, F.; Lee, C.S. Role of titanium dioxide (TiO_2) structural design/morphology in photocatalytic air purification. *Appl. Catal. B-Environ.* **2020**, *269*, 118735. [CrossRef]
5. Kania, A.; Szindler, M.M.; Szindler, M. Structure and corrosion behavior of TiO_2 thin films deposited by ALD on a biomedical magnesium alloy. *Coatings* **2021**, *11*, 70. [CrossRef]
6. Muthaiah, V.M.; Indrakumar, S.; Suwas, S.; Chatterjee, K. Surface engineering of additively manufactured titanium alloys for enhanced clinical performance of biomedical implants: A review of recent development. *Bioprinting* **2022**, *20*, e00180. [CrossRef]
7. Armakovic, S.J.; Savanovic, M.M.; Armakovic, S. Titanium dioxide as the most used photocatalyst for water purification: An overview. *Catalysts* **2023**, *13*, 26. [CrossRef]
8. Shih, P.C.; Huang, C.H.; Chen, T.H.; Lai, L.W.; Lu, Y.S.; Liu, D.S. Enhancement on Photocatalytic Activity of an Amorphous Titanium Oxide Film with Nano-Textured Surface by Selective-Fluorination Etching Process. *Mater. Res. Bull.* **2014**, *52*, 177–182. [CrossRef]
9. Cesaria, M.; Scrimieri, L.; Torrisi, A.; Quarta, G.; Serra, A.; Manno, D.; Caricato, A.P.; Martino, M.; Calcagnile, L.; Velardi, L. Pulsed-laser deposition and photocatalytic activity of pure rutile and anatase TiO_2 films: Impact of single-phased target and deposition conditions. *Vacuum* **2022**, *202*, 111150. [CrossRef]
10. Kameya, Y.; Yamada, T. Titanium oxide nanoparticle coating of PMMA open flow channels for spontaneous water transport. *Colloid Surf. A-Physicochem. Eng. Asp.* **2022**, *655*, 130265. [CrossRef]
11. Lazaro-Navas, S.; Prashar, S.; Fajardo, M.; Gomez-Ruiz, S. Visible light-driven photocatalytic degradation of the organic pollutant methylene blue with hybrid palladium-fluorine-doped titanium oxide nanoparticles. *J. Nanopart. Res.* **2015**, *17*, 94. [CrossRef]
12. Mahmoud, M.S.; Ahmed, E.; Farghali, A.A.; Zaki, A.H.; Abdelghani, E.A.M.; Barakat, N.A.M. Influence of Mn, Cu, and Cd-doping for titanium oxide nanotubes on the photocatalytic activity toward water splitting under visible light irradiation. *Colloid Surf. A-Physicochem. Eng. Asp.* **2018**, *554*, 100–109. [CrossRef]
13. Laghaei, M.; Wang, Y.C.; Rashed, A.O.; Beladi, H.; Kong, L.X. Facile electrochemical anodisation for generating nanopores across visible light-responsive cerium-titanium oxide heterojunctions for environmental remediation. *J. Environ. Chem. Eng.* **2023**, *11*, 110341. [CrossRef]
14. Sass, D.T.; Mouele, E.S.M.; Ross, N. Nano silver-iron-reduced graphene oxide modified titanium dioxide photocatalytic remediation system for organic dye. *Environments* **2019**, *6*, 106. [CrossRef]
15. Chiang, Y.C.; Tseng, T.L. Characterization and electrochemical properties of Pt nanoparticles deposited on titanium oxide nanofibers. *Mater. Chem. Phys.* **2021**, *267*, 124700. [CrossRef]
16. Zhu, H.; Tan, J.; Qiu, J.; Wang, D.; Zhao, Z.; Lu, Z.; Huang, G.; Liu, X.; Mei, Y. Gold nanoparticles decorated titanium oxide nanotubes with enhanced antibacterial activity driven by photocatalytic memory effect. *Coatings* **2022**, *12*, 1351. [CrossRef]

17. Zhang, J.K.; You, K.S.; Huang, C.H.; Shih, P.J.; Liu, D.S. Investigations into the photocatalytic and antibacterial activity of the nitrogen-annealed titanium oxide/silver structure. *Coatings* **2022**, *12*, 1671. [CrossRef]
18. Chen, J.Z.; Chen, T.H.; Lai, L.W.; Li, P.Y.; Liu, H.W.; Hong, Y.Y.; Liu, D.S. Preparation and characterization of the surface photocatalytic activity with NiO/TiO_2 nanocomposite structure. *Materials* **2015**, *8*, 4273–4286. [CrossRef]
19. Kozak, M.; Mazierski, P.; Żebrowska, J.; Kobylański, M.; Klimczuk, T.; Lisowski, W.; Trykowski, G.; Nowaczyk, G.; Zaleska-Medynska, A. Electrochemically obtained TiO_2/Cu_xO_y nanotube arrays presenting a photocatalytic response in process of pollutants degradation and bacteria inactivation in aqueous phase. *Catalysts* **2018**, *8*, 237. [CrossRef]
20. Liang, R.; Wang, Y.W.; Qin, C.; Chen, X.H.; Ye, Z.Z.; Zhu, L.P. P-type cobalt phosphide composites (CoP–Co_2P) decorated on titanium oxide for enhanced noble-metal-free photocatalytic H_2 evolution activity. *Langmuir* **2021**, *37*, 3321–3330. [CrossRef]
21. Wilson, H.; VanRooij, A.; Jenewein, K.; Knöppel, J.; Kormányos, A.; Cherevko, S.; Sunde, S.; Erbe, A. Photocorrosion of n- and p-type semiconducting oxide-covered metals: Case studies of anodized titanium and copper. *Phys. Status Solidi A-Appl. Res.* **2022**, *219*, 2100852. [CrossRef]
22. Kim, T.W.; Ha, H.W.; Paek, M.J.; Hyun, S.H.; Choy, J.H.; Hwang, S.J. Unique phase transformation behavior and visible light photocatalytic activity of titanium oxide hybridized with copper oxide. *J. Mater. Chem.* **2010**, *20*, 3238–3245. [CrossRef]
23. Yurddaskal, M.; Dikici, T.; Celik, E. Effect of annealing temperature on the surface properties and photocatalytic efficiencies of Cu_2O/CuO structures obtained by thermal oxidation of Cu layer on titanium substrates. *Ceram. Int.* **2016**, *42*, 17749–17753. [CrossRef]
24. Sarac, M.F.; Ozturk, K.; Yatmaz, H.C. A facile two-step fabrication of titanium dioxide coated copper oxide nanowires with enhanced photocatalytic performance. *Mater. Charact.* **2020**, *159*, 110042. [CrossRef]
25. Wu, C.Y.; Chiang, B.S.; Chang, S.; Liu, D.S. Determination of photocatalytic activity in amorphous and crystalline titanium oxide films prepared using plasma-enhanced chemical vapor deposition. *Appl. Surf. Sci.* **2011**, *257*, 1893–1897. [CrossRef]
26. Baer, D.R.; Artyushkova, K.; Cohen, H.; Easton, C.D.; Engelhard, M.; Gengenbach, T.R.; Greczynski, G.; Mack, P.; Morgan, D.J.; Roberts, A. XPS guide: Charge neutralization and binding energy referencing for insulating samples. *J. Vac. Sci. Technol. A* **2020**, *38*, 031204. [CrossRef]
27. Greczynski, G.; Hultman, L. Binding energy referencing in X-ray photoelectron spectroscopy. *Nat. Rev. Mater.* **2025**, *10*, 62–78. [CrossRef]
28. Li, H.; Zhao, G.; Han, G.; Song, B. Hydrophilicity and photocatalysis of $Ti_{1-x}V_xO_2$ films prepared by sol-gel method. *Surf. Coat. Technol.* **2007**, *201*, 7615–7618. [CrossRef]
29. Sarkandi, A.F.; Montazer, M.; Harifi, T.; Rad, M.M. Innovative preparation of bacterial cellulose/silver nanocomposite hydrogels: In situ green synthesis, characterization, and antibacterial properties. *J. Appl. Polym. Sci.* **2020**, *138*, 49824. [CrossRef]
30. Steveson, M.; Arora, P.S.; Smart, R.S.C. XPS studies of low-temperature plasma-produced graded oxide-silicate-silica layers on titanium. *Surf. Interface Anal.* **1998**, *26*, 1027–1034. [CrossRef]
31. McCafferty, E.; Wightman, J.P. An X-ray photoelectron spectroscopy sputter profile study of the native air-formed oxide film on titanium. *Appl. Phys. Sci.* **1999**, *143*, 92–100. [CrossRef]
32. Zheng, S.K.; Wang, T.M.; Hao, W.C.; Shen, R. Improvement of photocatalytic activity of TiO_x thin film by Sn ion implantation. *Vacuum* **2002**, *65*, 155–159. [CrossRef]
33. Marino, C.E.B.; Nascente, P.A.P.; Biaggio, S.R.; Rocha-Filho, R.C.; Bocchi, N. XPS characterization of anodic titanium oxide films grown in phosphate buffer solutions. *Thin Solid Film.* **2004**, *468*, 109–112. [CrossRef]
34. Dorraj, M.; Alizadeh, M.; Sairi, N.A.; Basirum, W.J.; Goh, B.T.; Woi, P.M.; Alias, Y. Enhanced visible light photocatalytic activity of copper-doped titanium oxide-zinc oxide heterojunction for methyl orange degradation. *Appl. Surf. Sci.* **2017**, *414*, 251–261. [CrossRef]
35. Ratova, M.; Klaysri, R.; Praserthdam, P.; Kelly, P.J. Visible light active photocatalytic C-doped titanium dioxide films deposited via reactive pulsed DC magnetron co-sputtering: Properties and photocatalytic activity. *Vacuum* **2018**, *149*, 214–224. [CrossRef]
36. Wang, Y.; Wu, Y.; Yang, H.; Xue, X.; Liu, Z. Doping TiO_2 with boron or/and cerium elements: Effect on photocatalytic antimicrobial activity. *Vacuum* **2016**, *131*, 58–64. [CrossRef]
37. Xu, W.; Tang, H.; Zhou, N.; Zhang, Q.; Peng, B.; Shen, Y. Enhanced photocatalytic activity of TiO_2/Ag_2O heterojunctions by optimizing the separation of electric charges. *Vacuum* **2021**, *190*, 110283. [CrossRef]
38. Kirsch, P.D.; Ekerdt, J.D. Chemical and thermal reduction of thin films of copper (II) oxide and copper (I) oxide. *J. Appl. Phys.* **2001**, *90*, 4256–4264. [CrossRef]
39. Cornette, P.; Zanna, S.; Seyeux, A.; Costa, D.; Marcus, P. The native oxide film on a model aluminium-copper alloy studied by XPS and ToF-SIMS. *Corros. Sci.* **2020**, *174*, 108837. [CrossRef]
40. Alotaibi, A.M.; Williamson, B.A.D.; Sathasivam, S.; Kafizas, A.; Alqahtani, M.; Sotelo-Vazquez, C.; Buckeridge, J.; Wu, J.; Nair, S.P.; Scanlon, D.O.; et al. Enhanced photocatalytic and antibacterial ability of Cu-doped anatase TiO_2 thin films: Theory and experiment. *ACS Appl. Mater. Interfaces* **2020**, *12*, 15348–15361. [CrossRef]

41. Chen, W.; Xu, J.; Huang, F.; Zhao, C.; Cuan, Y.; Fang, Y.; Hu, J.; Yang, W.; Luo, Z.; Guo, Y. CO oxidation over CuO_x/TiO_2 catalyst: The importance of oxygen vacancies and Cu^+ species. *Appl. Surf. Sci.* **2023**, *618*, 156539. [CrossRef]
42. Lv, Z.; Ding, Y.; Kang, L.; Li, L.; Liu, X.Y.; Wang, A.; Zhang, T. Light-enhanced direct epoxidation of propylene by molecular oxygen over CuO_x/TiO_2 catalyst. *Acta Phys.-Chim. Sin.* **2025**, *41*, 100038. [CrossRef]
43. Klein, F.; Pinedo, R.; Hering, P.; Polity, A.; Janek, J.; Adelhelm, P. Reaction mechanism and surface film formation of conversion materials for lithium- and sodium-ion batteries: An XPS case study on sputtered copper oxide (CuO) thin film model electrodes. *J. Phys. Chem. C* **2016**, *120*, 1400–1414. [CrossRef]
44. Liu, L.; Li, W.; Xiong, Z.; Xia, D.; Yang, C.; Wang, W.; Sun, Y. Synergistic effect of iron and copper oxides on the formation of persistent chlorinated aromatics in iron ore sintering based on in situ XPS analysis. *J. Hazard. Mat.* **2019**, *366*, 202–209. [CrossRef]
45. Hayashida, K.; Tsuda, Y.; Yamada, T.; Yoshigoe, A.; Okada, M. Revisit of XPS studies of supersonic O_2 molecular adsorption on Cu(111): Copper oxides. *ACS Omega* **2021**, *6*, 26814–26820. [CrossRef]
46. Pawar, S.M.; Kim, J.; Inamdar, A.K.; Woo, H.; Jo, Y.; Pawar, B.S.; Cho, S.; Kim, H.; Im, H. Multi-functional reactively-sputtered copper oxide electrodes for supercapacitor and electro-catalyst in direct methanol fuel cell application. *Sci. Rep.* **2016**, *6*, 21310. [CrossRef]
47. Zhang, M.; Chen, Z.; Wang, Y.; Zhang, J.; Zheng, X.; Rao, D.; Han, X.; Zhong, C.; Hu, W.; Deng, Y. Enhanced light harvesting and electron-hole separation for efficient photocatalytic hydrogen evolution over Cu_7S_4-enwrapped Cu_2O nanocubes. *Appl. Catal. B Environ.* **2019**, *246*, 202–210. [CrossRef]
48. Mobarak, M.B.; Hossain, M.S.; Chowdhury, F.; Ahmed, S. Synthesis and characterization of CuO nanoparticles utilizing waste fish scale and exploitation of XRD peak profile analysis for approximating the structural parameters. *Arab. J. Chem.* **2022**, *15*, 104117. [CrossRef]
49. Janczarek, M.; Kowalska, E. On the origin of enhanced photocatalytic activity of copper-modified titania in the oxidative reactive system. *Catalysts* **2017**, *7*, 317. [CrossRef]
50. Sawicka-Chudy, P.; Sibinski, M.; Rybak-Wilusz, E.; Cholewa, M.; Wise, G.; Yavorskyi, R. Review of the development of copper oxides with titanium dioxide thin-film solar cells. *AIP Adv.* **2020**, *10*, 010701. [CrossRef]
51. Kim, S.C.; Tsuchiya, H.; Manaka, T.; Hanawa, T.; Fujimoto, S. Passive film formed on Ti and Cr in a phosphate buffer solution of pH 7. *J. Electrochem. Soc.* **2024**, *171*, 031506. [CrossRef]
52. Kim, G.; Back, H.; Kong, J.M.; Naseer, L.; Jeong, J.; Son, J.; Lee, J.J.; Kang, S.O.; Lee, K.H. Chemically engineered titanium oxide interconnecting layer for multijunction polymer solar cells. *Polymer* **2024**, *16*, 595. [CrossRef] [PubMed]
53. Khanna, K.; Sharma, A.; Ohri, P.; Bhardwaj, R.; Abd Allah, E.F.; Hashem, A.; Ahmad, P. Impact of plant growth promoting rhizobacteria in the orchestration of Lycopersicon esculentum Mill. Resistance to plant parasitic nematodes: A metabolomic approach to evaluate defense responses under field conditions. *Biomolecules* **2019**, *9*, 676. [CrossRef] [PubMed]
54. Devi, T.B.; Ahmaruzzaman, M. Facile synthesis of γGO/Ag@AgCl core-shells nanocomposite and their multifunctional efficacy as a photocatalyst and antimicrobial agent for decontamination of water. *J. Alloys Compd.* **2021**, *860*, 157988. [CrossRef]
55. Brillas, E. Progress of antibiotics removal from synthetic and real waters and wastewaters by persulfate-based advanced oxidation processes. *J. Environ. Chem. Eng.* **2023**, *11*, 111303. [CrossRef]
56. Zhang, C.H.; Liang, W.J.; Dou, B.J.; Zhu, Y.X.; Yan, N.N.; Zhang, Y.; Salleh, S.; Bin, F. Application insights of environmental catalysts: Synergistic effects of cellulose-based porogens and catalytic metal sites in toluene catalytic oxidation. *Fuel* **2024**, *367*, 131402. [CrossRef]
57. Hara, M.; Kondo, T.; Komoda, M.; Ikeda, S.; Shinohara, K.; Tanaka, A.; Kondo, J.N.; Domen, K. Cu_2O as a photocatalyst for overall water splitting under visible light irradiation. *Chem. Commun.* **1998**, *3*, 357–358. [CrossRef]

Disclaimer/Publisher's Note: The statements, opinions and data contained in all publications are solely those of the individual author(s) and contributor(s) and not of MDPI and/or the editor(s). MDPI and/or the editor(s) disclaim responsibility for any injury to people or property resulting from any ideas, methods, instructions or products referred to in the content.